AIAA JOURNAL
Vol. 40, No. 5, May 2002

Probabilistic Methods for Design Assessment of Reliability with Inspection

Y.-T. Wu,* M. P. Enright,† and H. R. Millwater‡
Southwest Research Institute, San Antonio, Texas 78238-5166

Conventional gas turbine rotor life prediction methodologies are based on nominal conditions that do not adequately account for material and manufacturing anomalies that can degrade the structural integrity of high-energy rotors. To account for these anomalies, the Rotor Integrity Subcommittee of the Aerospace Industries Association recommended adoption of a probabilistic damage tolerance approach to supplement the current safe-life methodology. The recommendation led to the development of a computer program called DARWIN™ that computes the probability of fracture as a function of flight cycles, considering random defect occurrence and location, random inspection schedules, and several other random variables. The probabilistic fatigue analysis methodology developed for DARWIN to address hard alpha material anomalies is presented. The capability of this computer program is demonstrated using several realistic rotor models provided by aircraft engine manufacturers. It is shown that the life approximation function and importance sampling methods significantly reduce computation time (nearly two orders of magnitude) compared to the Monte Carlo method. In addition, an optimal zone sampling strategy is presented that can minimize the total number of samples required to achieve a desired sampling accuracy result for a given confidence interval. This probabilistic methodology can be used to focus design efforts on variables that have the most influence on risk reduction.

Nomenclature

$a_{\max}$	=	maximum defect area
$a_{\min}$	=	minimum defect area
$D(a)$	=	expected number of defects of area a in W
d	=	defect size
F_i	=	failure event in zone i, where $i = 1, m$
F_{X_1}	=	defect size cumulative distribution function
$f(a)$	=	probability density function associated with defect of area a
f_x	=	joint probability density function of the random variables associated with P_f
$g(\boldsymbol{X}, \boldsymbol{Y}, t)$	=	fatigue failure limit state
$h(\boldsymbol{n})$	=	constraint function
i	=	zone number
j	=	zone number
K, $K(\boldsymbol{X}, \boldsymbol{Y}, t)$	=	stress intensity factor
K_C	=	fracture toughness
l	=	fatigue life random variable, cycles
l_{model}	=	predicted fatigue life based on established fatigue crack growth equations and algorithms
m	=	number of zones in disk
N	=	total number of samples
N_f	=	number of failures with inspection in domain Ω
N_Ω	=	number of samples in domain Ω
$\boldsymbol{n}$	=	vector containing n_i for all m zones
n_i	=	number of samples in zone i
P_{detected}	=	probability of detecting a defect from a population of defects
POD(a)	=	probability of detecting a defect with a size (area) greater than a
P_f	=	(total) disk probability of failure
$\hat{P}_f$	=	sampling-based estimate of P_f
p_i	=	(conditional) probability of failure of zone i given that a single defect is in zone i
$\bar{p}_i$	=	zone probability of failure without inspection
S_{σ_i}	=	sigma (standard deviation) sensitivity coefficient
s	=	stress random variable
s_{FEM}	=	estimated stress based on finite element analysis results at the location of the defect
t, t_i	=	inspection time, cycles
W	=	quantity of material associated with defect exceedance curve
$\boldsymbol{X}$	=	vector of input variables unrelated to inspections
X_i	=	continuous random variable
X_1	=	defect size random variable
X_2	=	stress multiplier random variable that accounts for errors in geometry and numerical (e.g., finite element) modeling
X_3	=	life scatter random variable
$\boldsymbol{Y}$	=	vector of input variables related to inspections
$Z(\boldsymbol{n})$	=	objective function of n_I
$Z_{\alpha/2}$	=	standard normal variate evaluated at $(1-\alpha)$ confidence level
γ	=	relative sampling error
δ_i	=	defect occurrence probability in zone i
λ	=	Lagrange multiplier
μ_i	=	mean of random variable i
σ_i	=	standard deviation associated with random variable i
σ_{p_f}	=	standard deviation of disk probability of failure
$\sigma_{\hat{p}_f}$	=	standard deviation of sampling-based disk probability of failure estimate
σ_{p_i}	=	standard deviation of zone probability of failure
$\phi\{\boldsymbol{n}, \lambda\}$	=	Lagrange function
Ω	=	failure domain (random variable space in which all the predicted lives are shorter than the design life)
$(1-\alpha)$	=	confidence level

Received 30 April 2001; revision received 1 August 2001; accepted for publication 13 September 2001.

*Staff Engineer, Materials Engineering Department. Member AIAA.
†Senior Research Engineer, Materials Engineering Department. Member AIAA.
‡Principal Engineer, Materials Engineering Department. Member AIAA.

Introduction

PREMIUM grade titanium alloys, formerly processed by double vacuum arc remelting (VAR) and now processed by triple

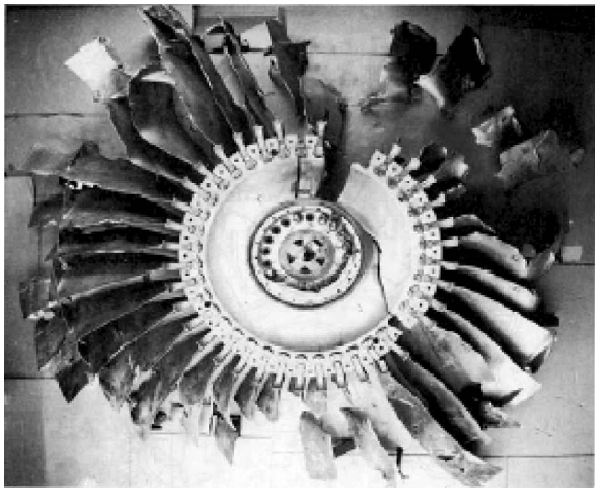

Fig. 1 Rare metallurgical anomalies can lead to uncontained engine failures.[1]

VAR, are used for fan and compressor rotors and disks in aircraft jet engines. Occasional upsets during processing can result in the formation of metallurgical anomalies referred to as hard alpha (HA). These anomalies are nitrogen-rich alpha titanium that are brittle and often have microcracks and microvoids associated with them. Although rare, these anomalies have led to uncontained engine failures (Fig. 1) that resulted in fatal accidents such as the incident at Sioux City Iowa in 1989. In a report issued by the Federal Aviation Administration (FAA) after the accident in Sioux City,[1] it was recommended that a probabilistic damage tolerance approach be implemented to explicitly address HA anomalies, with the objective of enhancing the conventional rotor life management methodology. The approach adopted and summarized in this paper is based on probabilistic fracture mechanics. This enhancement is intended to supplement, not replace, the current safe-life methodology.

The probabilistic damage tolerance code developed in this program for low-cycle fatigue of titanium rotors/disks containing HA anomalies is called DARWIN™. It was developed in collaboration with General Electric Aircraft Engines, Honeywell, Pratt and Whitney Aircraft (United Technologies), and Rolls–Royce.[2] DARWIN is a computer program that integrates finite element stress analysis, fracture mechanics analysis, nondestructive inspection simulation, and probabilistic analysis to assess the risk of rotor fracture. It computes the probability of fracture as a function of flight cycles, considering random defect occurrence and location, random inspection schedules, and several other random variables. Both Monte Carlo (MC) simulation and advanced fast integration methods are integral to the probabilistic driver. A fracture mechanics module, called Flight_Life,[3] is also incorporated into the code. In addition, a user-friendly graphical user interface is available to handle the otherwise difficult task of setting up the problem for analysis and viewing the results.[4]

The recent announcement of FAA advisory circular (AC) 33.14-1 (Ref. 5) adds a new damage tolerance element to the existing design and life management process for aircraft turbine rotors. Use of DARWIN is an acceptable method for complying with AC 33.14-1 and has the potential to reduce the uncontained rotor disk failure rate and to identify optimal inspection schedules.

This paper presents the probabilistic fatigue analysis methodology developed for DARWIN. The capability of this computer program is demonstrated using several realistic rotor models provided by aircraft engine manufacturers. It is shown that the life approximation function (LAF) and importance sampling (IS) methods significantly reduce computation time (nearly two orders of magnitude) compared to the MC method without a significant decrease in accuracy. Sensitivity analysis results indicate that, compared to the other random variables considered, initial defect size and stress variability have the most influence on lifetime failure probability. The extent of this influence is dependent on the relative coefficient of variation (COV) magnitudes among the key random variables. In addition, an optimal zone sampling strategy is presented that can significantly reduce the total number of samples required to achieve a desired sampling accuracy result for a given confidence interval. The efficient probabilistic methodology presented herein can be used to focus design efforts on variables that have the most influence on risk reduction.

Probabilistic Life Prediction Methodology

Failure Limit State

Given an initial defect in a rotor disk subjected to variable amplitude loading, the defect size d and stress intensity factor K increase with increasing number of flight cycles. Failure occurs when the maximum K exceeds the fracture toughness K_C:

$$g(\boldsymbol{X}, \boldsymbol{Y}, t) = K_C - K(\boldsymbol{X}, \boldsymbol{Y}, t) \leq 0 \tag{1}$$

where $g(\boldsymbol{X}, \boldsymbol{Y}, t)$ is dependent on t (flight cycles) and two general input variable vectors, $\boldsymbol{X}$ and $\boldsymbol{Y}$:

$$g(\boldsymbol{X}, \boldsymbol{Y}, t) = g(X_1, \ldots, X_n; Y_1, \ldots, Y_m; t) \tag{2}$$

A negative or zero $g(\boldsymbol{X}, \boldsymbol{Y}, t)$ represents a failure event.

The probability of failure is

$$P_f = P[g(\boldsymbol{X}, \boldsymbol{Y}, t) \leq 0] \tag{3}$$

Zone-Based Risk Integration Method

Metallurgical defects can be randomly distributed within a disk. To account for the uncertainty in the defect location, a zone-based risk integration approach is used. The disk is divided into a manageable number of zones of approximately equal risk (Fig. 2). The risk is computed in each zone, taking into account the zone defect occurrence probability δ_i, that is, the probability that a defect is present in a zone. The total risk for the disk is based on the sum of the risks in the individual zones.

The basis for the zone-based approach is a low occurrence rate associated with hard alpha defects. Define F_i as a failure event in zone i, $i = 1, m$. The disk risk P_f is the probability union of the zone F_i:

$$P_f = P[F_1 \cup F_2 \cup \cdots \cup F_m] \tag{4}$$

If the occurrence rate of significant defects, that is, defects with sizes that could cause failure, is small, such that, given a significant defect in a zone, the probability of having other significant defects in the same disk is negligible [i.e., for any two arbitrary zones i and j, $P(F_i \cap F_j)$ is small compared to $P(F_i)$ or $P(F_j)$, irrespective of the number of zones m], then Eq. (4) can be simplified as

$$P_f \approx \sum_{i=1}^{m} P[F_i] \tag{5}$$

which can be written as

$$P_f \approx \sum_{i=1}^{m} \delta_i \cdot p_i \tag{6}$$

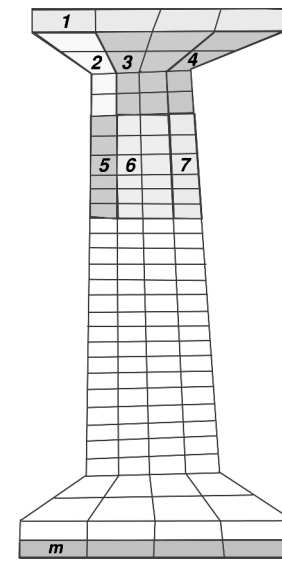

Fig. 2 DARWIN zone-based risk assessment method identifies failure critical regions in aircraft rotors.

where δ_i is the defect occurrence probability in zone i and p_i is the (conditional) probability of failure of zone i given that a single defect is in zone i.

A major advantage of the zone-based approach is that it allows zone-dependent $\boldsymbol{X}$ and $\boldsymbol{Y}$ variables and defect occurrence probabilities. Because these variables can differ significantly throughout a typical disk (for example, stress, crack growth rate, inspection method, among others), the approach can provide a more realistic life estimate (provided that the disk is subdivided into a sufficient number of zones). In addition, the approach allows the analysis to be focused on significant zones, thereby allowing the probabilistic analysis to be done faster and more effectively.

Random Variables

In considering the structural integrity of a titanium rotor disk containing HA anomalies, the potential $\boldsymbol{X}$ random variables include defect size and location, stress, and material properties. The time and effectiveness of the inspections are among the potential $\boldsymbol{Y}$ random variables. The effectiveness of an inspection can be characterized by its probability of detection (POD) distribution.

Three $\boldsymbol{X}$ random variables are considered in the current methodology, including defect size X_1 and two others related to the stress X_2 and life X_3 models. An exceedance curve[6] for a quantity of material, for example, $W = 1 \times 10^6$ lb (2.2×10^6 kg), is used to characterize the defect occurrence rate and defect area distribution (Fig. 3). A defect cumulative distribution function is defined as follows:

$$F_{X_1}(a) = \begin{cases} 0, & a < a_{\min} \\ 1 - \dfrac{D(a) - D(a_{\max})}{D(a_{\min}) - D(a_{\max})}, & a_{\min} \le a \le a_{\max} \\ 1, & a > a_{\max} \end{cases} \tag{7}$$

A practical stress uncertainty model is defined as follows[7]:

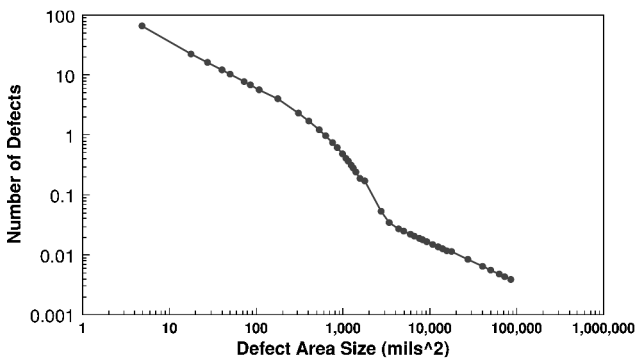

Fig. 3 Defect exceedance curve (10^6 lb) (2.2×10^6 kg) for titanium rotor disk materials (1 mil^2 = 1550 mm^2).[6]

$$s = X_2 \cdot s_{\text{FEM}} \tag{8}$$

where s_{FEM} is the estimated stress based on finite element analysis results at the location of the defect.

Similarly, a practical stochastic life model is defined as

$$l = X_3 \cdot l_{\text{model}} \tag{9}$$

where l_{model} is the predicted fatigue life based on established fatigue crack growth equations and algorithms.

The $\boldsymbol{Y}$ random variables are the inspection (shop visit) times and the POD. Inspection time t_i is modeled as a random variable. The probability of detecting a defect from a population of defects, P_{detected}, is

$$P_{\text{detected}} = \int_0^\infty \text{POD}(a) \cdot f(a)\, \text{d}a \tag{10}$$

where POD (a) is the probability of detecting a defect with a size (area) greater than a and $f(a)$ is the probability density function associated with a defect of area a.

Computational Methods for Reliability-Based Life Prediction Under Inspection

Several sampling-based probabilistic analysis methods can be used to predict the life of disks subjected to periodic inspection. MC simulation provides accurate results (the accuracy is dependent on the failure probability, confidence interval, and number of random samples) but is relatively inefficient because the failure limit state must be evaluated for each random sample using a fatigue crack growth algorithm. The LAF creates deterministic life and grown area arrays for a family of initial defects. During MC simulation, the failure limit state is evaluated for each random sample using values interpolated from the deterministic arrays, thereby improving computational efficiency. The IS method focuses analysis on the initial conditions (defect size and other random variables) that would result in lives shorter than the specified design life. This approach reduces the size of the analysis region and may be significantly more efficient than MC simulation. An overview of the IS methodology for predicting fatigue life of components subjected to periodic inspections is shown in Fig. 4.

MC Simulation

MC random simulation is time consuming but is the easiest and most robust method to implement for complicated problems. This method has the most flexibility for future expansion and can be used to provide reference solutions to verify other faster methods.

The computation time associated with deterministic life prediction, that is, cycles to failure, can vary considerably depending on the geometry and fracture mechanics solution used. For a fatigue crack growth prediction based on a one-dimensional stress gradient, the CPU time may be relatively small, for example, on the order

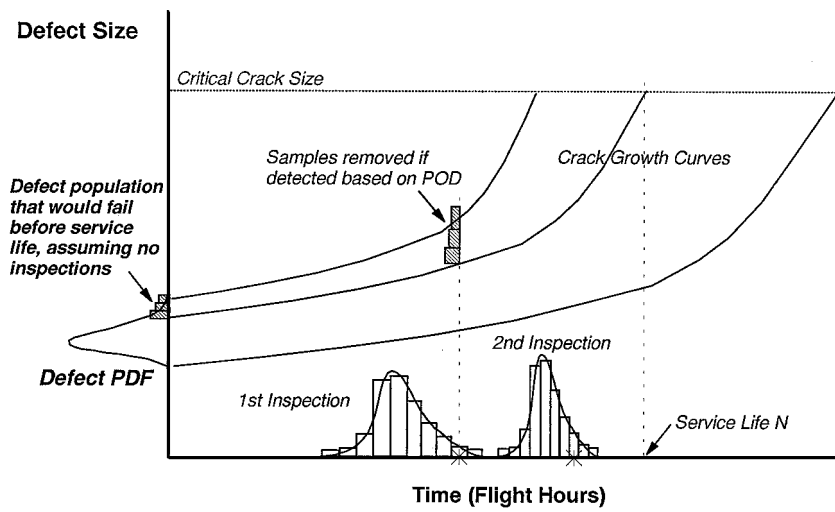

Fig. 4 Overview of importance sampling methodology for probabilistic fatigue life prediction of components subjected to multiple inspections.

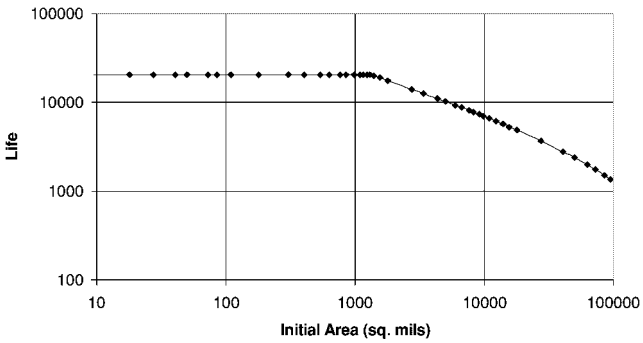

Fig. 5 Life vs initial defect area curve used for LAF life prediction ($1\ \text{mil}^2 = 1550\ \text{mm}^2$).

of 1s or less when using a Hewlett-Packard 700 series workstation or its equivalent. However, when MC simulation is used, a separate crack growth computation must be performed for each initial defect sample. Because the number of MC samples needed to satisfy accuracy requirements is typically on the order of 10^4–10^6 or greater, the total CPU time required to complete these computations can be significant. Also, identification of the optimal inspection time typically requires many additional risk computations.

LAF

The LAF computes the life (cycles to failure) and grown area for a given initial defect area using two internal arrays that are created before MC simulation. The first array contains life vs initial defect area for a number of discrete initial defect areas (based on the initial defect distribution). The second array contains grown area vs cycles for a number of discrete initial defect areas (also based on the initial defect distribution). The LAF uses interpolation on a log–log scale to compute the cycles to failure and grown area for an arbitrary initial defect and inspection time. A typical life vs initial defect area graph created using this method is shown in Fig. 5. (Note that, in this example, the life vs area curve shown is truncated at a design life of 20,000 cycles.) The advantage of this approach is that, during MC sampling, estimates for the life and crack area are obtained directly from the internal arrays, which can significantly improve computational efficiency.

Importance Sampling

This hybrid method combines numerical integration with random sampling, focusing samples in the failure region. It includes the following steps:

1) Calculate the zone probability of failure without inspection, $\bar{p}_i$, using numerical integration.

2) Generate, in the following sequence, a selected number of realizations of life scatter, stress multiplier, and initial defect size in the failure domain Ω.

a) Randomly generate life scatter according to its probability density function (PDF) in the failure region.

b) Randomly generate a stress multiplier according to its PDF in the failure region, given the life scatter.

c) Randomly generate a defect according to its PDF in the failure region, given the life scatter and the stress multiplier.

3) With the use of the samples, perform a MC simulation of crack growth and inspection processes to determine the number of disks removed by inspection.

4) Compute the conditional zone probability of failure (with inspection), p_i:

$$p_i = \bar{p}_i(N_f/N_\Omega) \tag{11}$$

The approach is significantly faster than the MC method, particularly when $\bar{p}_i$ is very small.

Sampling-Based Risk Sensitivity Analysis

The sensitivity of the disk failure probability P_f with respect to changes in the standard deviation σ_i of a random variable i can be evaluated from[8]

$$S_{\sigma_i} = \frac{\partial P_f/P_f}{\partial \sigma_i/\sigma_i} = \int_\Omega \cdots \int \frac{\sigma_i}{P_f}\frac{\partial f_x}{f_x \partial \sigma_i} f_x \, \mathrm{d}x \tag{12}$$

If all variables are independent and normally distributed, the sigma sensitivity coefficient becomes[8]

$$S_{\sigma_i} = E\left\{[(X_i - \mu_i)/\sigma_i]^2 - 1\right\}_\Omega \tag{13}$$

Optimize Number of Samples in Each Zone

The error associated with sampling-based probabilistic methods, for example, MC simulation, is directly related to the failure probability and the number of samples. For both the MC and IS methods, the zone failure probability p_i is estimated using a random sample of size n_i. Because the failure probability can vary significantly from zone to zone, the error associated with zone failure probability predictions can also vary if the number of samples in each zone is a constant. To achieve a consistent error, each zone needs a different sample size, depending on both δ_i and p_i. Based on Eq. (6), the approach used[9,10] to determine the optimal sample size for each zone is based on minimizing the variance $\sigma^2_{p_f}$ of the disk probability of failure:

$$\sigma^2_{p_f} \approx \sum_{i=1}^{m} \delta_i^2 \sigma^2_{p_i} \tag{14}$$

For a sample size n_i, probability p_i has a binomial distribution, which, for large n_i, can be approximated by a normal distribution[11] with mean p_i and variance $p_i(1-p_i)/n_i$. The total number of samples for the disk is equal to the sum of the samples in all of the zones, that is,

$$N = \sum_{i=1}^{m} n_i$$

Values of n_i that minimize σ_{p_f} can be identified using a standard optimization formulation:

$$\text{minimize} \quad Z(\boldsymbol{n}) = \sum_{i=1}^{m} \frac{\delta_i^2 p_i(1-p_i)}{n_i}$$

$$\text{subject to} \quad N = \sum_{i=1}^{m} n_i \tag{15}$$

Using the Lagrange-multiplier method, the objective function becomes

$$\phi\{\boldsymbol{n}, \lambda\} = \sum_{i=1}^{m} \frac{\delta_i^2 p_i(1-p_i)}{n_i} + \lambda h(\boldsymbol{n}) \tag{16}$$

$$= \sum_{i=1}^{m} \frac{\delta_i^2 p_i(1-p_i)}{n_i} + \lambda\left(N - \sum_{i=1}^{m} n_i\right) \tag{17}$$

At the optimum, the following conditions must be satisfied:

$$\frac{\partial \phi}{\partial n_i} = 0, \qquad i = 1, 2, \ldots, m \tag{18}$$

$$\frac{\partial \phi}{\partial \lambda} = 0 \tag{19}$$

When Eqs. (18) and (19) are applied to Eq. (17),

$$\frac{\partial \phi}{\partial n_i} = \frac{-\delta_i^2 p_i(1-p_i)}{n_i^2} - \lambda = 0, \qquad i = 1, 2, \ldots, m \tag{20}$$

$$\frac{\partial \phi}{\partial \lambda} = N - \sum_{i=1}^{m} n_i = 0 \tag{21}$$

From Eq. (20) it follows that

$$n_i^2 = \delta_i^2 p_i(1-p_i)/-\lambda \tag{22}$$

$$n_i = \delta_i \sqrt{p_i(1-p_i)}\Big/\sqrt{-\lambda} \tag{23}$$

When Eq. (23) is substituted into Eq. (21),

$$N - \sum_{i=1}^{m} \frac{\delta_i \sqrt{p_i(1-p_i)}}{\sqrt{-\lambda}} = 0 \tag{24}$$

$$\sqrt{-\lambda} = \frac{1}{N} \sum_{i=1}^{m} \delta_i \sqrt{p_i(1-p_i)} \tag{25}$$

When Eq. (25) is substituted into Eq. (23), the following result is obtained:

$$n_i = N \frac{\delta_i \sqrt{p_i(1-p_i)}}{\sum_{i=1}^{m} \delta_i \sqrt{p_i(1-p_i)}} \tag{26}$$

Equation (26) shows that the optimal n_i is proportional to $N\delta_i\sqrt{[p_i(1-p_i)]}$. In the extreme cases, n_i approaches zero as δ_i (or p_i) approaches 0 (or p_i approaches 1).

The value of N can be determined by relating it to a desired sampling accuracy. When Eqs. (15) and (22) are used, the variance of P_f can be written as

$$\sigma_{p_f}^2 = \sum_{i=1}^{m} \frac{\delta_i^2 p_i(1-p_i)}{n_i} = \sum_{i=1}^{m} -\lambda n_i = -\lambda N \tag{27}$$

which becomes

$$\sigma_{p_f} = \sqrt{-\lambda N} = \frac{1}{\sqrt{N}} \sum_{i=1}^{m} \delta_i \sqrt{p_i(1-p_i)} \tag{28}$$

or

$$\sqrt{N} = \sum_{i=1}^{m} \frac{\delta_i \sqrt{p_i(1-p_i)}}{\sigma_{p_f}} \tag{29}$$

For a large number of samples N, the binomial distribution can be approximated as a normal distribution with the following mean and variance:

$$E(\hat{P}_f) = P_f \tag{30}$$

$$\sigma_{\hat{P}_f}^2 \approx (1/N)\hat{P}_f(1-\hat{P}_f) \tag{31}$$

The $(1-\alpha)$ confidence interval associated with P_f is defined as

$$P\left[-Z_{\alpha/2} < \frac{\hat{P}_f - P_f}{\sqrt{\hat{P}_f(1-\hat{P}_f)/N}} \le Z_{\alpha/2}\right] = 1-\alpha \tag{32}$$

Define the sampling error as

$$\gamma = (\hat{P}_f - P_f)/P_f \tag{33}$$

From Eqs. (31–33) it follows that, at the upper and lower confidence bounds,

$$\sigma_{\hat{P}_f} = \gamma P_f / Z_{\alpha/2} \tag{34}$$

When Eqs. (29) and (34) are combined,

$$\sqrt{N} = \frac{Z_{\alpha/2}}{\gamma P_f} \sum_{i=1}^{m} \delta_i \sqrt{p_i \cdot (1-p_i)} \tag{35}$$

Equation (35) can be used to compute the number of samples required to predict P_f for a given relative error and confidence. Optimal n_i values can then be identified using Eq. (26).

Numerical Illustration of Probabilistic Computational Methods

Consider the titanium ring disk model shown in Fig. 6 (AC base case). The design life of the disk is 20,000 flight cycles. The maximum disk speed during each flight cycle is 6000 rpm. A 50-MPa external pressure load is applied to the outer surface of the disk to simulate blade loading. Internal stresses and temperatures are determined using finite element analysis.

The initial defect area and POD are shown in Figs. 3 and 7, respectively. Main descriptors for the stress scatter, life scatter, and inspection time random variables are indicated in Table 1. Additional details regarding this model and associated data are presented elsewhere.[2]

Table 1 AC base case random variables

Variable	Median	COV, %	Distribution
Stress scatter	1.0	0–30	Lognormal
Life scatter	1.0	0–30	Lognormal
Inspection time	10,000 cycles	0–30	Normal

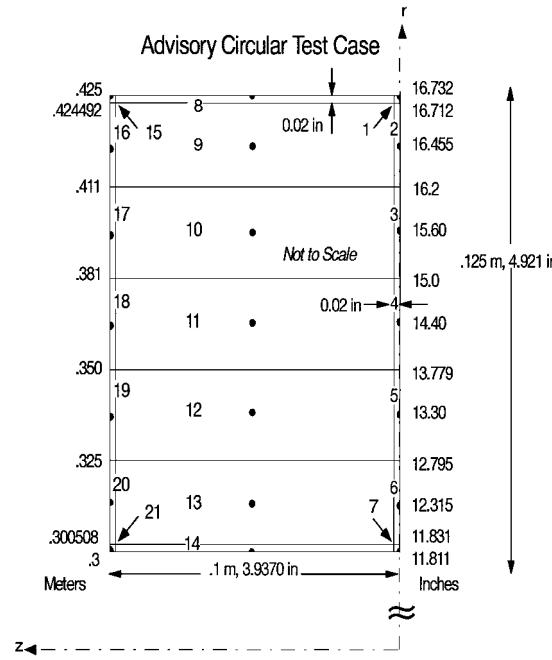

Fig. 6 Example rotor disk model: zone definition.

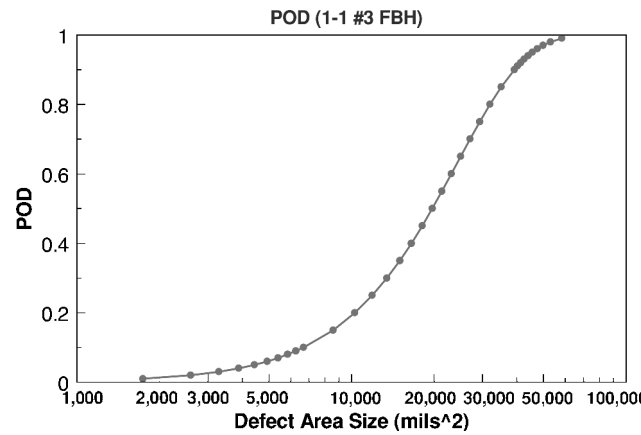

Fig. 7 POD curve[5] used for numerical example (1 mil^2 = 1550 mm^2).

Zone Discretization

The disk is divided into 21 zones (Fig. 6). The material properties, stresses, and temperatures within each zone are approximately constant. Subsurface defects are located in the geometric center of the interior zones, and surface defects are located on the outer surfaces of the exterior zones. For design applications, it may be preferable to place defects at the minimum-life locations to achieve conservative solutions. It is assumed that the probability of occurrence of a single defect in each zone is very small, and the probability of occurrence of two significant defects, that is, defects with associated fatigue lives shorter than the design life, within the same disk is negligible (consistent with the observed defect occurrence rate in titanium disks).

Influence of Inspection

In practice, detailed in-service inspections of an aircraft rotor disk may not occur at predetermined intervals but are performed when

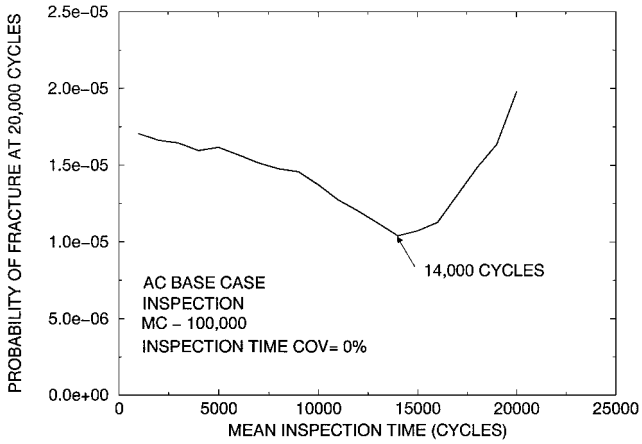

Fig. 8 Influence of mean inspection time on lifetime failure probability.

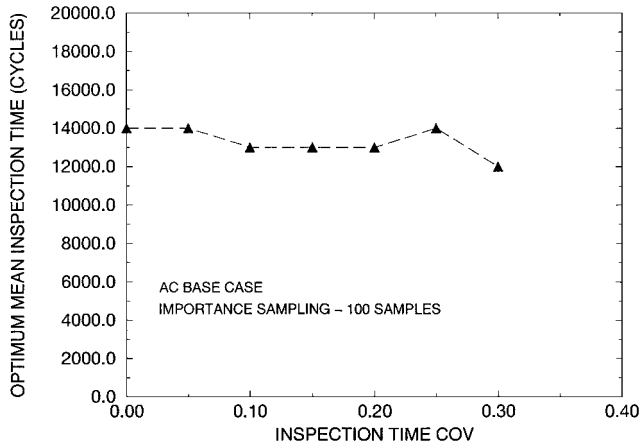

Fig. 9 Influence of inspection time COV on optimum mean inspection time.

the engine is in the shop for other maintenance activities. Consequently, the inspection time can vary considerably. To account for this variability, the inspection time is modeled as a random variable. It is assumed that all disks with detected defects are removed. For this illustrative example, the inspection time is modeled as a normally distributed random variable with mean value equal to 50% of the design life (10,000 cycles) and inspection time COV range 0–30% (Table 1).

In Fig. 8, the effect of varying the mean inspection time is shown for a single deterministic inspection, that is, inspection time COV = 0%. For this example, the inspection time can have a significant influence on the disk failure probability P_f at the end of the design life, that is, probability of fracture at 20,000 cycles. P_f reaches a minimum value when the inspection is performed at approximately 70% of the design life (14,000 cycles). Note that the P_f gradient, that is, the change in P_f with respect to inspection time, is asymmetric about the optimum value and increases significantly as the inspection time approaches the design life. Consequently, the influence of inspection time variability on P_f becomes more significant near the end of the service life.

The inspection time COV has some influence on the value of the optimum mean inspection time that minimizes the lifetime failure probability P_f. In Fig. 9, it can be observed that the optimum mean inspection time varies from 12,000 to 14,000 cycles for inspection time COVs ranging from 0 to 30%.

In Fig. 10, the influence of inspection time COV on lifetime failure probability P_f is shown for a mean inspection time of 10,000 cycles. Also shown are failure probabilities for the optimum mean inspection times associated with inspection time COVs ranging from 0 to 30%. It can be observed that P_f is relatively insensitive to inspection time COV if the inspection is not performed at the optimum time. However, if the optimum mean inspection time is used, P_f is sensitive to inspection time COV and increases with increasing

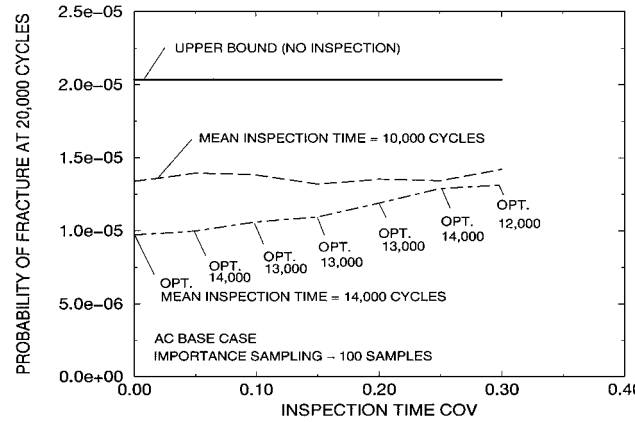

Fig. 10 Influence of inspection time COV on lifetime failure probability.

COV values. The results shown in Figs. 9 and 10 suggest that the optimal mean inspection time is dependent on inspection time COV.

For deterministic inspection time, that is, inspection time COV = 0, the P_f obtained at the optimal mean inspection time represents a lower bound, that is, minimum P_f for all values of inspection time COV. This lower bound value is important because it defines the maximum influence of inspection on failure probability reduction.

Probabilistic Computational Methods Results Comparison

A comparison of conditional failure probability results for the IS and MC simulation methods is shown in Fig. 11. It can be observed that IS results (200–500 samples) match remarkably well with MC (1×10^6 samples).

A comparison of the speed and accuracy of the MC, LAF, and IS methods was performed using DARWIN for several rotor disk models (including two realistic finite element models provided by industry). Results are shown in Figs. 12–15 (see Refs. 10 and 12 for further details).

In Fig. 12, failure probability results are shown for three rotor disk models (AC base case and industry models I and II). The computational method and number of samples used in each simulation is indicated in Fig. 12. Although the overall failure probability results are different for the three models (as expected), the influence of computational method on failure probability is relatively small for a given rotor disk model.

Computation times (Hewlett–Packard 700 series CPU times) associated with the MC, LAF, and IS methods are shown in Fig. 13 for three rotor disk models. It can be observed that, for a given model and number of samples, the computation times associated with the LAF and IS methods are significantly lower compared to those associated with MC. For industry model II, computation time was reduced from 2000 to 80 min and 25 min for the LAF and IS methods, respectively, that is, up to nearly two orders of magnitude or more with a similar degree of accuracy. For a given computational method, the differences in the computation times shown for each of the three models are primarily due to the model complexity, for example, number of zones, fracture mechanics methods, number of load blocks, among others.

Computational error associated with the MC, LAF, and IS methods is shown in Fig. 14 for the AC base case. Error results are based relative to a MC simulation result (1.5×10^6 samples for the disk). For a given seed value and number of samples, the error associated with the MC and LAF methods is very similar. Also note that the error associated with the IS method using 100 or 400 samples per zone is substantially lower than that of the MC and LAF methods using 10,000 samples per zone. This suggests that, for this example problem, the computational efficiency associated with the LAF and IS methods is achieved without a significant decrease in accuracy.

A comparison of the efficiency and accuracy associated with the MC, LAF, and IS methods is shown in Fig. 15 for the AC base case. For this example, it can be observed that IS provides both the lowest error magnitude and the lowest computation time compared to MC and LAF for the range of parameters considered.

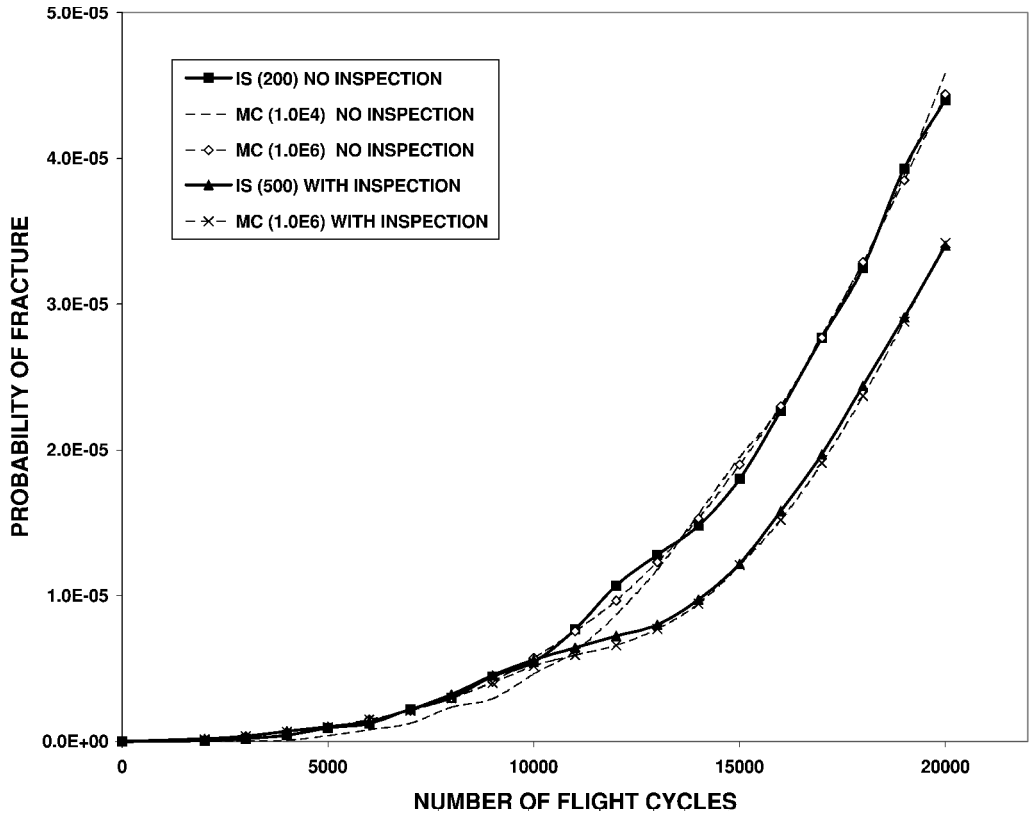

Fig. 11 Comparison of importance sampling and MC results.

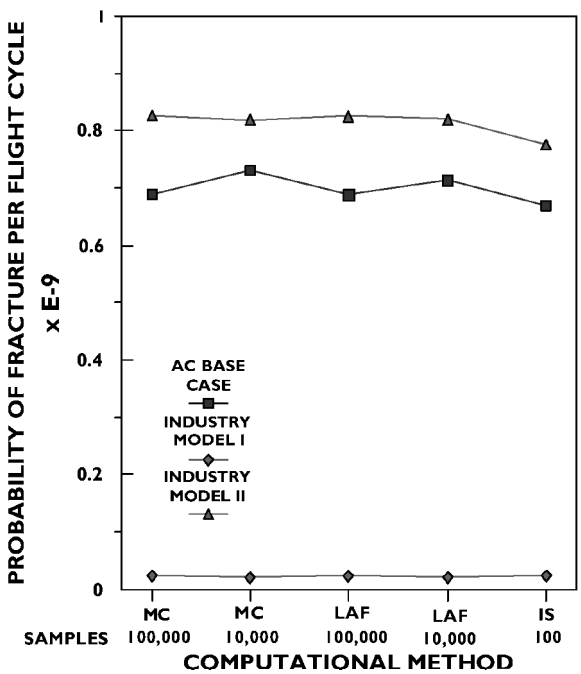

Fig. 12 Comparison of computational method results for several structural models.

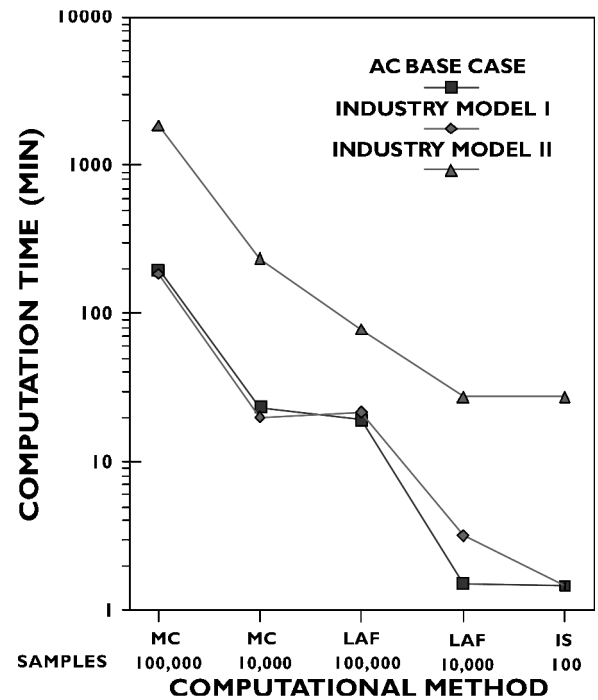

Fig. 13 Computational method efficiency comparison.

Risk Sensitivity Analysis

A parametric sensitivity analysis was performed to compare the influences of stress, life scatter, and inspection time variability on lifetime failure probability P_f for the AC base case. In Fig. 16 it can be observed that stress COV has a dominant effect on P_f. In fact, for this example, the P_f associated with 10% stress COV is larger than the failure probabilities associated with 30% COV for life scatter and inspection time. This illustrates that a reduction in the stress COV can have more influence on reducing P_f compared to the life scatter and inspection time COVs.

The sampling based risk sensitivity analysis method outlined in Eqs. (12) and (13) is illustrated for the stress scatter, life scatter, and defect size random variables for a critical zone (AC base case, zone 13). The main descriptors for these variables are indicated in Table 2. The defect distribution was approximated based on a curve fit of the defect exceedance curve shown in Fig. 3. The curve fit was focused on the right tail, that is, largest defect size, and the distribution was assumed to be lognormal.

Using 100 IS samples that were within the failure region, that is, life $<$ 20,000 cycles if no inspection is performed, the sensitivity

Table 2 Main descriptors of variables used for sampling-based sensitivity analysis

Variable	Median	COV, %	Distribution
Stress scatter	1.0	10	Lognormal
Life scatter	1.0	10–50	Lognormal
Defect distribution	90 mil^2	110	Lognormal

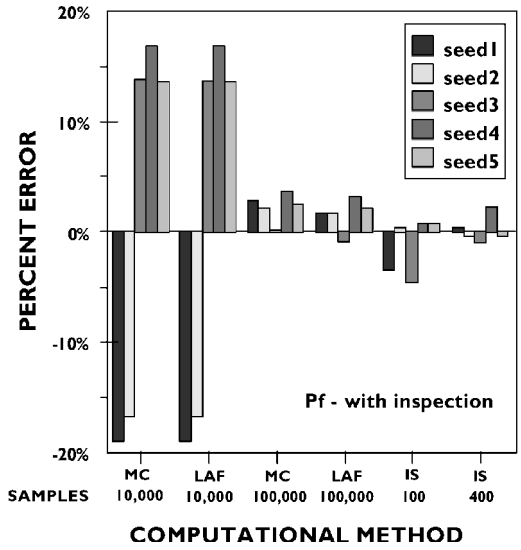

Fig. 14 Computational method error comparison.

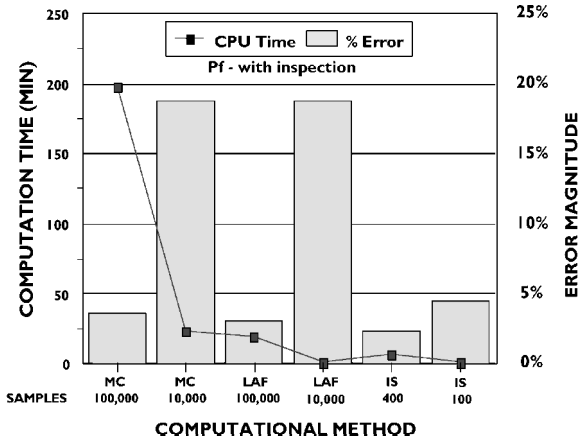

Fig. 15 Importance sampling and life approximation algorithms significantly reduce computation time and error associated with MC simulation.

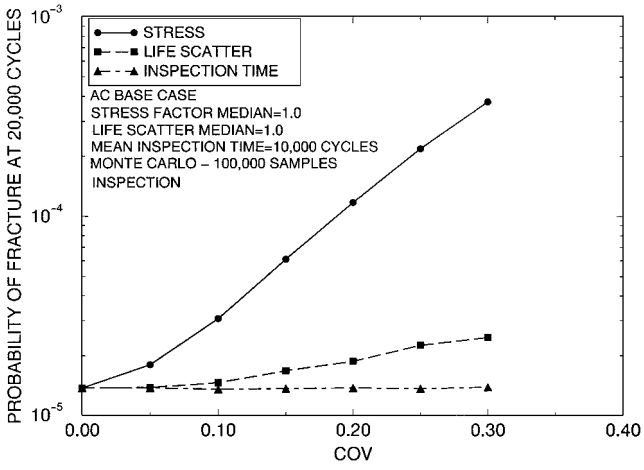

Fig. 16 Parametric sensitivity comparison: influences of stress, life scatter, and inspection time COVs on lifetime failure probability.

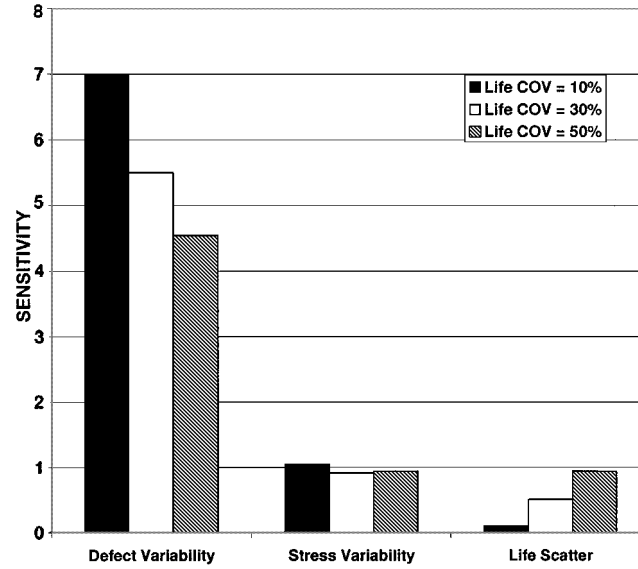

Fig. 17 Sampling-based risk sensitivity analysis used to identify and rank influential probabilistic variables.

of the probability of failure P_f with respect to the changes in the standard deviations of the stress scatter, life scatter, and defect size was computed using Eq. (13).

The result, shown in Fig. 17, suggests that the defect size is the most dominant random variable, as expected. Assuming a COV of 10% for both life scatter and stress scatter, the result suggests that life scatter has a minimal contribution. However, if the life scatter COV is increased to 50%, its influence on P_f is comparable to that of stress scatter. This information is useful for assessing the need for more accurate data/probabilistic models for the stress and life variables.

Zone Sample Size Optimization

The earlier comparisons of the probabilistic methods suggest that a systematic approach for selecting the zone sample size is needed. This section compares the optimal sampling strategy (strategy 3) to two other zone sample allocation strategies to illustrate the benefit of the zone-based optimal sampling approach.

For strategy 1, the total number of samples is based on the variance of zone failure probability. Combine Eqs. (30–32) and solve for N:

$$N = \frac{Z^2_{\alpha/2}}{\gamma^2}\frac{(1-P_f)}{P_f} = \frac{Z^2_{\alpha/2}}{\gamma^2}\frac{\left(1-\sum \delta_i p_i\right)}{\sum \delta_i p_i} \tag{36}$$

For a single zone, Eq. (36) becomes

$$n_i = \frac{Z^2_{\alpha/2}}{\gamma^2}\frac{(1-\delta_i p_i)}{\delta_i p_i} \tag{37}$$

where the total number of samples for the disk is

$$N = \sum_{i=1}^{m} n_i \tag{38}$$

This strategy considers only the error within individual zones. It can be very inefficient for zones with relatively small δ_i and p_i values because a large number of samples is required to compute failure probabilities that may have little influence on the disk failure probability.

For strategy 2, the total number of samples is based on the variance of the disk failure probability. The total number of samples for the disk is computed using Eq. (36). The number of samples in each zone is a fraction of the disk zones, for example,

$$n_i = N/m, \qquad N = \left(Z^2_{\alpha/2}/\gamma^2\right)[(1-P_f)/P_f] \tag{39}$$

This strategy does not consider the influences of δ_i and p_i on the number of samples in each zone. Compared to the other strategies, it is easier to implement but less efficient.

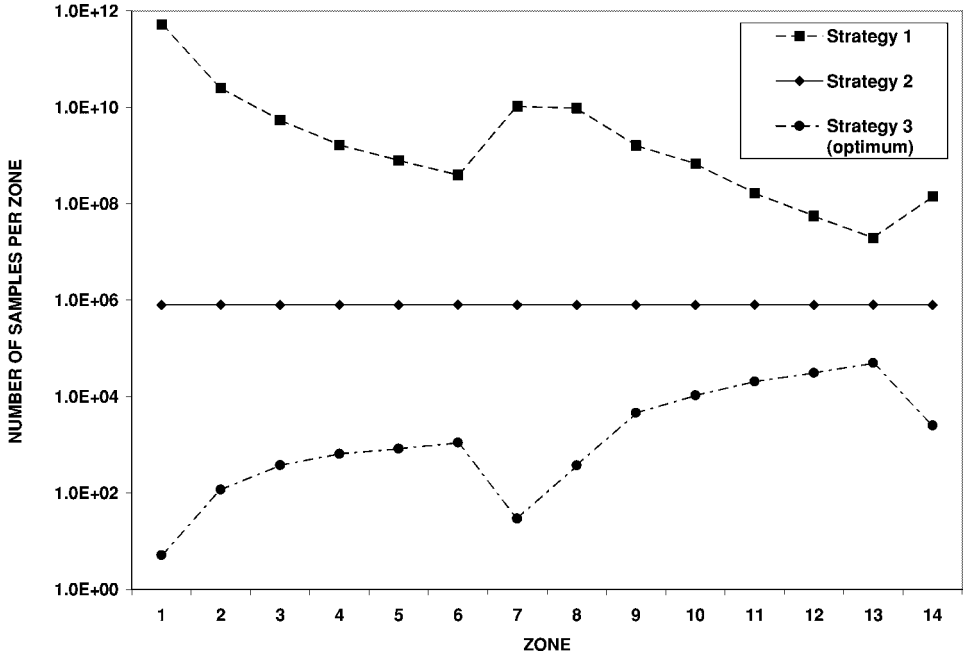

Fig. 18 Comparison of three zone sample allocation strategies (10% sampling error at 95% confidence).

Table 3 AC base case zone failure probabilities

Zone	δ_i	p_i	$\delta_i^* p_i$
1	8.937$E-$07	8.141$E-$04	7.276$E-$10
2	2.243$E-$05	6.757$E-$04	1.515$E-$08
3	5.003$E-$05	1.407$E-$03	7.042$E-$08
4	4.618$E-$05	4.955$E-$03	2.288$E-$07
5	3.554$E-$05	1.355$E-$02	4.818$E-$07
6	3.192$E-$05	3.047$E-$02	9.728$E-$07
7	6.318$E-$07	5.800$E-$02	3.664$E-$08
8	8.714$E-$05	4.547$E-$04	3.962$E-$08
9	2.187$E-$03	1.087$E-$04	2.377$E-$07
10	4.878$E-$03	1.159$E-$04	5.653$E-$07
11	4.503$E-$03	5.130$E-$04	2.310$E-$06
12	3.466$E-$03	1.982$E-$03	6.870$E-$06
13	3.113$E-$03	6.303$E-$03	1.962$E-$05
14	6.160$E-$05	4.379$E-$02	2.697$E-$06
Total	——	——	3.414$E-$05

Table 4 Total number of samples required for 10% error at 95% confidence

Strategy	Number of samples
1	5.85$E+$11
2	1.13$E+$7
3	1.22$E+$5

Strategy 3 has the optimum samples per zone. From Eqs. (26) and (35)

$$n_i = N\frac{\delta_i\sqrt{p_i(1-p_i)}}{\sum_{i=1}^{m}\delta_i\sqrt{p_i(1-p_i)}}$$

$$N = \frac{Z_{\alpha/2}^2}{\gamma^2 P_f^2}\left[\sum_{i=1}^{m}\delta_i\sqrt{p_i\cdot(1-p_i)}\right]^2 \tag{40}$$

The three strategies were applied to life prediction of the (21 zone) AC base case (Fig. 6). Zone failure probabilities (obtained using MC simulation) are indicated in Table 3. A comparison of the number of samples per zone required for 10% sampling error at 95% confidence is shown in Fig. 18. For each zone, the number of samples required for the optimal strategy is significantly lower than the other strategies considered. For strategy 1, it can be observed that zones with relatively low $\delta_i p_i$ values have the most samples, whereas for strategy 3, zones with relatively high $\delta_i p_i$ values have the most samples. A comparison of the total number of MC samples required for these strategies (10% sampling error at 95% confidence) is indicated in Table 4. It can be observed that the total number of samples required for the optimal sampling strategy is significantly lower (nearly two orders of magnitude lower) than the other sampling strategies considered. In addition, the total number of samples required to achieve the same result can be significantly reduced if importance sampling is used.

Conclusions

An overview of the DARWIN probabilistic fatigue life prediction methodology was presented, including descriptions of the algorithms used for risk and risk sensitivity predictions. The computational accuracy and efficiency of this methodology is illustrated for several aircraft titanium turbine rotor models. For the range of fatigue random variables and disk geometries considered, the following observations can be made:

1) As expected, the mean inspection time can have a large influence on lifetime failure probability. However, inspection time variability, that is, COV, does not appear to have a significant impact on P_f, particularly if the mean inspection time is not at the optimal time.

2) Optimal mean inspection time depends on the inspection time COV. P_f approaches a lower bound value as inspection time COV approaches 0, representing the maximum influence of inspection on failure probability reduction.

3) Relative to life scatter and stress scatter, the defect size has a dominant effect on lifetime failure probability. The extent of this influence is dependent on the relative COV magnitudes among these three key random variables.

4) Compared to life scatter and inspection time variability, the stress COV has the most influence on lifetime failure probability. Reducing the stress or stress variation, if possible, is an effective way of reducing P_f, perhaps even more effective than implementing inspection.

5) Compared to the MC method, the LAF and IS methods significantly reduce computation time without a significant decrease in accuracy. For one of the rotor models provided by industry, computation time was reduced nearly two orders of magnitude for the IS method.

6) The optimal zone sampling strategy can significantly reduce the total number of disk samples required to achieve a desired sampling error result for a given confidence. For the example problem presented, the total number of samples associated with the optimal

strategy was nearly two orders of magnitude lower than the other sampling strategies considered. The number of samples can be further reduced if importance sampling is used.

Most of these conclusions are based on an idealized rotor disk for a specific geometry, load condition, defect distribution, and POD. Results obtained for in-service turbine rotor disks under different assumptions may differ from the results presented in this study.

Acknowledgments

This work was performed as part of the Titanium Rotor Materials Design (TRMD) project, an ongoing effort supported by the Federal Aviation Administration under Cooperative Agreement 95-G-041 and Grant 99-G-016. The ongoing contributions of the Rotor Integrity Subcommittee of the Aerospace Industries Association and the TRMD Steering Committee are also gratefully acknowledged.

References

[1]"Aircraft Accident Report—United Airlines Flight 232 McDonnell Douglas DC-10-10 Sioux Gateway Airport, Sioux City, Iowa, 19 July 1989," National Transportation Safety Board, Rept. NTSB/AAR-90/06, Washington, DC, Nov. 1990.

[2]"Turbine Rotor Material Design—Final Report," Southwest Research Inst., AlliedSignal, General Electric Aircraft Engines, Pratt and Whitney Aircraft (United Technologies), Rolls–Royce, and Scientific Forming Technologies; Federal Aviation Administration, Rept. DOT/FAA/AR-00/64, Washington, DC, Dec. 2000.

[3]McClung, R. C., Leverant, G. R., Wu, Y.-T., Millwater, H. R., Chell, G. G., Kuhlman, C. J., Lee, Y.-D., Riha, D. S., Johns, S. R., and McKeighan, P. C., "Development of a Probabilistic Design System for Gas Turbine Rotor Integrity," *Fatigue'99: The Seventh International Fatigue Conference*, Beijing, 1999, pp. 2655–2660.

[4]Millwater, H. R., Fitch, S., Wu, Y.-T., Riha, D. S., Enright, M. P., Leverant, G. R., McClung, R. C., Kuhlman, C. J., Chell, G. G., and Lee, Y.-D., "A Probabilistically-Based Damage Tolerance Analysis Computer Program for Hard Alpha Anomalies in Titanium Rotors," *Proceedings of the 45th ASME International Gas Turbine and Aeroengine Technical Congress*, American Society of Mechanical Engineers, Fairfield, NJ, 2000, pp. 1–7.

[5]"Advisory Circular—Damage Tolerance for High Energy Turbine Engine Rotors," U.S. Dept. of Transportation, Federal Aviation Administration, Rept. AC 33.14-1, Washington, DC, Jan. 2001.

[6]Aerospace Industries Association Rotor Integrity Subcommittee, "The Development of Anomaly Distributions for Aircraft Engine Titanium Disk Alloys," *Proceedings of the 38th Structures, Structural Dynamics, and Materials Conference*, AIAA, Reston, VA, 1997, pp. 2543–2553.

[7]Wu, Y.-T., "An Efficient Method for Reliability Analysis of Structures Subjected to In-Service Inspections," *Proceedings of the 13th ASCE Engineering Mechanics Division Conference*, American Society of Civil Engineers, Reston, VA, 1999, pp. 1–6.

[8]Wu, Y.-T., "Computational Methods for Efficient Structural Reliability and Reliability Sensitivity Analysis," *AIAA Journal*, Vol. 32, No. 8, 1994, pp. 1717–1723.

[9]Wu, Y.-T., Millwater, H. R., and Enright, M. P., "Efficient and Accurate Methods for Probabilistic Analysis of Titanium Rotors," *Proceedings of the 8th ASCE Specialty Conference on Probabilistic Mechanics and Structural Reliability*, [CD-ROM Proceedings Paper PMC2000-221], 2000.

[10]Wu, Y.-T., Enright, M. P., McClung, R. C., Millwater, H., and Leverant, G. R., "Probabilistic Methods for Design Assessment of Reliability with Inspection (DARWIN™)," *Proceedings of the 41st Structures, Structural Dynamics, and Materials Conference*, AIAA, Reston, VA, 2000, pp. 1–9.

[11]Ang, A. H.-S., and Tang, W. H., *Probability Concepts in Engineering Planning and Design*, Wiley, New York, 1975, pp. 252, 253.

[12]Enright, M. P., and Wu, Y.-T., "Probabilistic Fatigue Life Sensitivity Analysis of Titanium Rotors," *Proceedings of the 41st Structures, Structural Dynamics, and Materials Conference*, AIAA, Reston, VA, 2000, pp. 1–9.

E. Livne
Associate Editor